Journal of Sound and Vibration (2000) **238**(4), 575–594
doi:10.1006/jsvi.2000.3090, available online at http://www.idealibrary.com on IDEAL®

A THEORY OF REACTIVE CONTROL OF LOW-FREQUENCY DUCT NOISE

L. HUANG

Department of Mechanical Engineering, The Hong Kong Polytechnic University, Kowloon, Hong Kong

(*Received* 21 *July* 1999, *and in final form* 19 *April* 2000)

A theoretical prediction is undertaken for low-frequency duct noise control by a compact reactive muffler. The muffler achieves a pressure-release condition over a broad frequency band (from near zero to the first cut-on frequency of the duct) by four flush-mounted pistons, one on each duct wall, with a structure to fluid mass ratio of the order of unity. The concept of a magnetic device is introduced to allow the stiffness of the system to be made sufficiently small, leading to a high transmission loss near the DC frequency. Interactions among the pistons yield negative virtual mass which neutralizes the structural inertia. The inertia neutralization is nearly perfect over a wide frequency band, so that the high transmission loss extends to the first cut-on frequency of the duct. The near-field analysis reveals that the negative virtual mass derives from the plane wave mode of sound radiation due to the mirror effect of the opposite duct wall, an effect which can be maximized by the pairing of pistons on the two opposing walls. For relatively heavy pistons a minimum transmission loss of 14 dB may be obtained for plane waves, while that of relatively compact and light pistons could exceed 30 dB. The effects of residual system stiffness required by the system stability, and of structural damping are shown to be insignificant except for a narrow band near the DC frequency.

1. INTRODUCTION

Low-frequency noise is very annoying and difficult to control. Typical sources include domestic air conditioning systems and public transport vehicles. Measures of dissipative noise control are ineffective while most traditional, reactive mufflers, such as expansion chambers of various forms, are either intrusive to flow or bulky [1]. Resonators can be made compact and relatively non-intrusive, but they work well only for narrow bands around the discrete resonance frequencies [2]. This paper explores theoretically the possibility of extending the effective bandwidth of a resonator-type device resembling a side-branch Helmholtz resonator.

In a Helmholtz resonator, the air in the neck contains most of the kinetic energy during oscillation and the cavity stores the potential energy. The system has a resonance frequency at which oscillation becomes self-sustained. Zero acoustic pressure at the mouth of the oscillator is maintained, which means a complete reflection of grazing incident waves in the duct. If impedance is defined as the ratio of excess pressure at the mouth to the velocity of flow through the neck, it vanishes at the resonance frequency. But for frequencies slightly different, it increases sharply. In other words, either heavy or stiff systems have little response to incident waves. The spectrum of transmission loss (TL henceforth) is narrow. It is possible to use some adaptive techniques to tune automatically the resonator geometry in response to the changing frequency of a tonal noise [3], but obviously it would be much better if the bandwidth of the device can be extended with a purely passive set-up.

0022-460X/00/490575 + 20 $35.00/0

In principle, active controlling devices perform much better in dealing with broadband and low-frequency noise, and there have been experimental successes in dealing with duct noise problems since the 1980s [4, 5]. But judging from recent reviews on the topic by Hansen [6], there is still some way to go before the technology of active noise control becomes mature and cost-effective for popular use. It is, therefore, still beneficial to explore alternatives in the framework of passive control for the low-frequency noise.

What we seek to achieve is to diminish both inertia and stiffness of the resonator, so that the pressure-release condition, or zero impedance, may be maintained over a certain band of frequencies instead of at discrete frequencies. To do so, we need to introduce negative stiffness and negative inertia of some sort, which is clearly difficult with conventional tools. We find that, with a proper acoustic arrangement (to be explained in later sections), a negative inertia can be achieved within the domain of mechanics. But to achieve negative stiffness by mechanical means is far more difficult. To extend our scope of control, we introduce the concept of stiffness adjustment by magnetic attraction force. The concept is illustrated in Figure 1 through a ferromagnetic membrane, but the formulation will be based on a more simplified model in which the effect of magnetic force is represented by a lumped parameter. Inevitably, the introduction of the membrane adds to the system inertia, but it is shown later that this inertia can be counter-balanced by the negative acoustic inertia.

As shown in Figure 1, the membrane may be clamped at its edges and is separated from a permanent magnet by an air gap of depth h. Forces resisting the displacement of the membrane originate from the membrane bending stiffness, tensile stress and the reaction of air in the cavity. The force promoting the displacement of the membrane is the magnetic attraction force, which increases when the membrane is drawn into the cavity, and *vice versa*. Such a change in the attraction force gives rise to a negative stiffness for the membrane vibration. Given the static magnetic force per unit area as $F = B(h + \eta)^{-2}$, where B is proportional to the magnetic strength (flux intensity) and η is the membrane displacement, a negative stiffness K_{mag} is achieved by the magnetic force, illustrated as follows:

$$K_{mag} = \mathrm{d}F/\mathrm{d}\eta \propto -2Bh^{-3}.$$

Details of implementation is the topic of our on-going experimental studies. In what follows, we tentatively assume that the factor of h^{-3} gives us so much control over K_{mag} that we can balance a large range of mechanical spring stiffness, K_{mech}, to achieve the infinitesimal total structural stiffness $(K_{mech} + K_{mag}) \to 0$.

Since the noise-induced displacement is normally small, the non-linearity of the distance dependence in $F \propto h^{-2}$ should not pose much problem for stiffness matching. But there are other concerns for the configuration of Figure 1. Strictly speaking, the magnetic force exerted by the magnet is not uniform over the membrane, and even the average force may not have the usual spatial dependence of h^{-2}. But we argue that, in principle, such quantitative details do not invalidate the concept of the negative stiffness. As a first step, we postpone the modelling of the dynamics of any specific design, such as that shown in Figure 1. Instead, we concentrate on the acoustics of the interaction between a compact vibrating surface and its surrounding fluid. Since our focus is on the low-frequency noise, the vibrating surface is acoustically compact and can be represented by a piston. Of course, such an approximation will have problems with the sharp edges when there is flow. The entire issue of the effect of flow is also postponed to future studies, but a few comments are in order here with respect to the possibility of flow-induced instability of the membrane

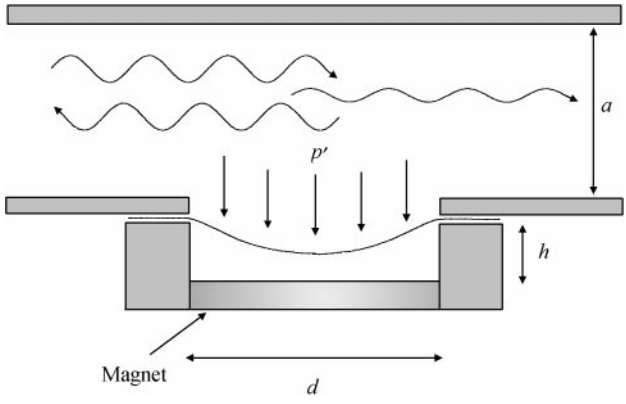

Figure 1. Schematic design of magnetic mechanism for neutralizing structural stiffness.

structure. When the flow reaches a certain limit, a thin membrane will be subject to a large static suction force of the steady flow. But such a force can be balanced by a suitable degree of vacuum in the air cavity below the membrane. The question of static divergence is still a valid one considering the effect of flow perturbation inside the channel. The system must have a positive total stiffness to maintain its stability, and the unsteady flow has a negative contribution to the total stiffness. Apart from static divergence, there is also a possibility of dynamic instability known as flutter. Instability of panel structures was studied extensively by Dowell [7], but the more relevant work for this case may be found from a theory of piston instability by Howe [8] who concluded that there was indeed a possibility of energy transfer from the vortical wake of flow separation at the trailing edge of a sharp-edged piston to piston vibration. A membrane structure like that shown in Figure 1 is compact enough to be modelled as a piston acoustically, but it may not possess an aerodynamic feature of vortex-shedding wake at the clamped edge. In any event, a sufficiently strong damping mechanism can be built into the structure to prevent flutter. In short, given a certain total stiffness margin, as well as a structural damping mechanism, it is unlikely that the structure will experience instability with a moderate flow in the channel. The effects of such stiffness margin and structural damping are investigated and the results are shown towards the end of this paper. The last but certainly not the least issue which is left to future studies is the forced structural vibration by flow turbulence.

In passing, it is also noted that the problem of "break-out" noise from air-conditioning ducts [9] originates from the strong noise–wall interaction, but such leaking of noise from within the duct is unintended. Significant noise leaking occurs under certain coincidence conditions in the low-frequency range. Deliberate use of such fluid–structure interaction is seen in the so-called membrane absorbers, mainly in the context of building acoustics [10–13]. The spectrum of noise reduction by membrane absorbers is mostly narrow-banded, but the pursuit of membrane-type sound absorbers has taken other forms such as spermeable membranes [14], as well as particle-loaded coatings [15] which have shown some broadband performance.

In what follows, we first analyze the fluid loading on a vibrating piston. The emphasis is on the physical interpretation of results for further exploitation of sound–piston interaction. We find that, with appropriate pairing of pistons, the fluid loading presents negative virtual mass which may effectively neutralize the structural inertia. A brief version of this study is presented elsewhere [16].

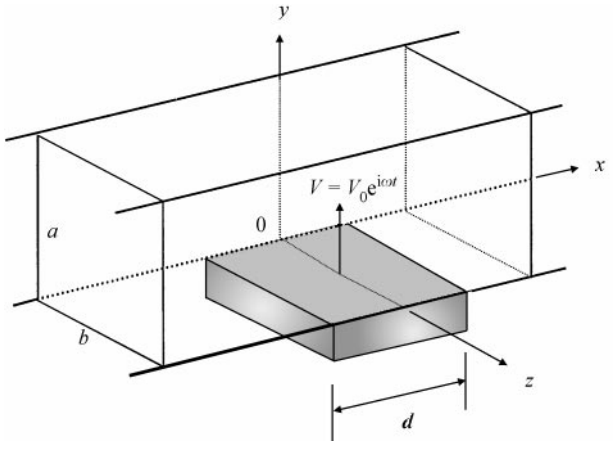

Figure 2. Configuration of wave generation by a flush-mounted piston.

2. WAVES GENERATED BY A FLUSH-MOUNTED PISTON

The mathematical problem of wave reflection and scattering by a flush-mounted piston shown in Figure 2 can be considered in three steps. First, the piston is tactically assumed to be rigid and the incident waves are allowed to pass without alteration. The fact that the piston does respond to the wave loading is considered in the second step, in which waves radiated by a specified heaving motion are calculated and the radiation loading on the piston is found. The left travelling wave represents the reflection while the right one is superimposed on the incident wave to form the transmitted wave. The superimposition is expected to be destructive causing positive TL. The actual amplitude and phase of the piston vibration are then resolved in the last step by the coupled dynamics involving (a) the pressure force from the incident wave, (b) the radiation fluid-loading from the piston vibration, and (c) the intrinsic structural forces of inertia, spring restoring force and structural damping. In this section, we study the radiation fluid-loading (b) for a given piston motion.

2.1. GENERAL WAVE FIELD

As shown in Figure 2, a flush-mounted piston vibrates at velocity $V = V_0 e^{i\omega t}$, where ω is the angular velocity and V_0 the amplitude. The axial dimension of the piston is d and the piston occupies the whole depth b of the rectangular duct of height a. The duct is rigid and infinite in its axial extent. The origin of the x-axis coincides with the centre of the piston. The pressure wave generated by a volume source on the surface S can be calculated in terms of the acoustic mode for a rigid duct, and is well-known [17]:

$$p(x, y, z, t) = \sum_{mn} \rho_0 c_{mn} \psi_{mn}(y, z) \frac{1}{2ab} \iint_S \psi^*_{mn}(y', z') V(x', y', z', t) \times [\mathrm{H}(x - x') e^{-i\omega(x-x')/c_{mn}} + \mathrm{H}(x' - x) e^{i\omega(x-x')/c_{mn}}] \, \mathrm{d}S', \tag{1}$$

where the source strength $V(x', y', z', t) = V$ is constant on the entire piston surface located on $y' = 0$, ρ_0 is the fluid density, c_0 is the isentropic speed of sound, H is the Heaviside function, c_{mn} is the (complex) modal wave speed defined as

$$\left(\frac{c_0}{c_{mn}}\right)^2 = 1 - \left(\frac{\omega_{mn}}{\omega}\right)^2, \quad \left(\frac{\omega_{mn}}{c_0}\right)^2 = \left(\frac{m\pi}{a}\right)^2 + \left(\frac{n\pi}{b}\right)^2,$$

ψ_{mn} is the normalized modal function

$$\psi_{mn}(y, z) = \sqrt{(2 - \delta_{0m})(2 - \delta_{0n})} \cos\left(\frac{m\pi y}{a}\right) \cos\left(\frac{n\pi z}{b}\right),$$

ψ^*_{mn} is the complex conjugate of ψ_{mn} ($\psi^*_{mn} = \psi_{mn}$ in this case) and δ_{ij} is the Kronecker delta function which becomes unity when its two subscripts are equal, $i = j$. Equation (1) satisfies (a) the homogeneous wave (Helmholtz) equation, $(\nabla^2 + \omega^2/c_0^2)p = 0$, everywhere except at the source surface, (b) the radiation conditions at $|x| \to \infty$, and (c) the source-observer reciprocity principle. Alternatively, one could start with Green's function for a baffled piston, which will end up with Hankel functions, and add the effect of the mirror image piston. But we adopt the method of direct modal expansion because it simplifies the necessary physical interpretations.

For the piston of Figure 2, the source element is $\mathrm{d}S' = \mathrm{d}x'\,\mathrm{d}z'$ and the z'-integration in equation (1) is done as follows:

$$\int_0^b \cos\left(\frac{n\pi z'}{b}\right) \mathrm{d}z' = b\,\frac{\sin(n\pi)}{n\pi} = \begin{cases} b, & n = 0, \\ 0, & n \neq 0. \end{cases}$$

This implies that there is no lateral mode other than the plane one, $n = 0$, and the pressure field is two-dimensional. For this reason we will drop the subscript n and variable z, e.g., $c_{m0} \to c_m$, $p(x, y, z, t) \to p(x, y, t)$. For the axial integration, we treat two regions separately. For the source region, $|x| \leqslant d/2$, we have

$$\int_{-d/2}^{x} \mathrm{e}^{-\mathrm{i}\omega(x - x')/c_m} \mathrm{d}x' + \int_{x}^{+d/2} \mathrm{e}^{\mathrm{i}\omega(x - x')/c_m} \mathrm{d}x' = 2\,\frac{c_m}{\mathrm{i}\omega}\left[1 - \mathrm{e}^{-\mathrm{i}\omega d/2c_m} \cos\left(\frac{\omega x}{c_m}\right)\right],$$

so the pressure becomes

$$p(|x| < d/2, y, t) = \sum_{m=0}^{\infty} \rho_0 c_m V (2 - \delta_{0m}) \times \cos\left(\frac{m\pi y}{a}\right) \frac{c_m}{\mathrm{i}\omega a}\left[1 - \mathrm{e}^{-\mathrm{i}\omega d/2c_m} \cos\left(\frac{\omega x}{c_m}\right)\right]. \tag{2}$$

If the excitation frequency is below the first cut-on frequency based on the duct height,

$$\omega < \omega_1 = \pi c_0/a,$$

equation (2) is conveniently separated into plane and evanescent waves

$$\frac{p(|x| \leqslant d/2, y, t)}{\rho_0 c_0 V} = \frac{c_0}{\mathrm{i}\omega a}\left[1 - \mathrm{e}^{-\mathrm{i}\omega d/2c_0} \cos\left(\frac{\omega x}{c_0}\right)\right] + \mathrm{i} \sum_{m=1}^{\infty} 2\,\frac{|c_m|^2}{\omega a c_0} \cos\left(\frac{m\pi y}{a}\right)\left[1 - \mathrm{e}^{-\omega d/2|c_m|} \cosh\left(\frac{\omega x}{|c_m|}\right)\right]. \tag{3}$$

Note that for $m = 1, 2, 3, \ldots$, $c_m = \mathrm{i}|c_m|$ and $\cos(\mathrm{i}\omega) = \cosh(w)$ has been applied. For the outer region, $|x| > d/2$, the axial integration is different:

$$\left.\begin{aligned} x > +d/2\text{:} & \int_{-d/2}^{+d/2} \tfrac{1}{2}\mathrm{e}^{-\mathrm{i}\omega(x-x')/c_m}\,\mathrm{d}x' \\ x > -d/2\text{:} & \int_{-d/2}^{+d/2} \tfrac{1}{2}\mathrm{e}^{+\mathrm{i}\omega(x-x')/c_m}\,\mathrm{d}x' \end{aligned}\right\} = \frac{c_m}{\omega}\sin\left(\frac{\omega d}{2c_m}\right)\mathrm{e}^{-\mathrm{i}\omega|x|/c_m}$$

and the pressure is

$$\frac{p(|x| > d/2, y, t)}{\rho_0 c_0 V} = \sum_{m=0}^{\infty}(2 - \delta_{0m})\cos\left(\frac{m\pi y}{a}\right)\frac{c_m^2}{\omega a c_0}\sin\left(\frac{\omega d}{2c_m}\right)\mathrm{e}^{-\mathrm{i}\omega|x|/c_m}$$

in general but

$$\begin{aligned}\frac{p(|x| > d/2, y, t)}{\rho_0 c_0 V} = {} & \frac{c_0}{\omega a}\sin\left(\frac{\omega d}{2c_0}\right)\mathrm{e}^{-\mathrm{i}\omega|x|/c_0} \\ & - \mathrm{i}\sum_{m=1}^{\infty} 2\cos\left(\frac{m\pi y}{a}\right)\frac{|c_m|^2}{\omega a c_0}\sinh\left(\frac{\omega d}{2|c_m|}\right)\mathrm{e}^{-\omega|x|/|c_m|}\end{aligned} \tag{4}$$

for the special case of low-frequency excitation, $\omega < \pi c_0/a$, for which the identity $\sin(\mathrm{i}w) = \mathrm{i}\sinh(w)$ has been used.

2.2. FLUID-LOADING OF A VIBRATING PISTON

The average radiation pressure acting on the piston itself may be found and expressed in the form $\bar{p} = \rho_0 c_0 V Z$ where $Z = R + \mathrm{i}X$ is the ratio of specific radiation impedance (simply impedance henceforth), R is the real part called resistance, and X is the imaginary part or reactance. Z is calculated from equation (2) by setting $y = 0$,

$$\begin{aligned} Z = \frac{1}{d}\int_{-d/2}^{+d/2}\frac{p(x, 0, t)}{\rho_0 c_0 V}\,\mathrm{d}x = {} & \frac{c_0}{\mathrm{i}\omega a}\left[1 - \mathrm{e}^{-\mathrm{i}\omega d/2c_0}\frac{\sin(\omega d/2c_0)}{(\omega d/2c_0)}\right] \\ & + \mathrm{i}\sum_{m=1}^{\infty} 2\frac{|c_m|^2}{\omega a c_0}\left[1 - \mathrm{e}^{-\omega d/2|c_m|}\frac{\sinh(\omega d/2|c_m|)}{(\omega d/2|c_m|)}\right].\end{aligned}$$

For later convenience, we define the following dimensionless parameters:

$$\alpha = \frac{d}{a}, \qquad \theta_m = \frac{\omega d}{2|c_m|}, \qquad f = \frac{\omega}{\omega_1}, \qquad \varpi = \frac{\omega a}{c_0} = \pi f. \tag{5}$$

Note that α becomes the piston aspect ratio (d/b) if the duct cross-section is square. f is the normalized frequency, which will be simply referred to as frequency, while ϖ is the normalized angular frequency. The radiation impedance may be re-written as

$$Z = \sum_{m=0}^{\infty} Z_m = R + \mathrm{i}X, \qquad X = \sum_{m=0}^{\infty} X_m,$$

$$R = \mathrm{Re}(Z_0) = \frac{\alpha}{2}\frac{\sin^2\theta_0}{\theta_0^2},$$

$$X_0 = -\frac{\alpha}{2\theta_0}\left(1 - \frac{\sin 2\theta_0}{2\theta_0}\right), \tag{6}$$

$$X_m = \frac{\alpha}{\theta_m}\frac{|c_m|}{c_0}\left(1 - \frac{1 - \mathrm{e}^{-2\theta_m}}{2\theta_m}\right).$$

The behaviour of the evanescent wave loading, $X_{m>0}$, as $m \to \infty$ is analyzed as follows:

$$\omega_m = \frac{m\pi c_0}{a}, \qquad \frac{c_0}{|c_m|} = \sqrt{\left(\frac{\omega_m}{\omega}\right)^2 - 1} \to \frac{m\lambda_0}{2a}, \qquad \lambda_0 = \frac{2\pi c_0}{\omega},$$

$$\theta_m = \frac{\omega d}{2|c_m|} \to \frac{\pi}{2}\alpha m, \qquad X_m \to \frac{4a}{\pi\lambda_0} \times \frac{1}{m^2}.$$

The convergence of the reactance series $\sum X_m$ should be rapid.

Contributions to the impedance from the plane wave, $Z_0 = R + \mathrm{i}X_0$, and the evanescent waves, $X_{m>0}$, are plotted separately in Figure 3 for $\alpha = 1$.

The range of excitation frequency is $f \in (0, 1)$. Several observations are made.

1. As shown in Figure 3(a), the radiation resistance R decreases with frequency. This is caused by the destructive interference of waves radiated by different parts of the piston. It will be shown later that this decrease contributes to the rapid fall of TL when the frequency exceeds that of piston resonance.
2. Comparing the magnitude of $X_{m>0}$ in Figure 3(b) and that of X_0 shown in Figure 3(a), we find that the main contribution to the total reactance, $\sum_{m=0}^{\infty} X_m$, comes from the evanescent waves for the particular example of $\alpha = 1$. For the part of evanescent waves, the first mode dominates over the sum of all the rest. As frequency $f \to 1$, the reactance from the first mode has the following asymptotic behaviour:

$$\frac{c_0}{|c_1|} = \frac{f}{\sqrt{1 - f^2}} \to \infty, \qquad \theta_1 \to 0, \qquad X_1 \to \frac{\alpha}{\sqrt{2(1 - f)}} \to \infty.$$

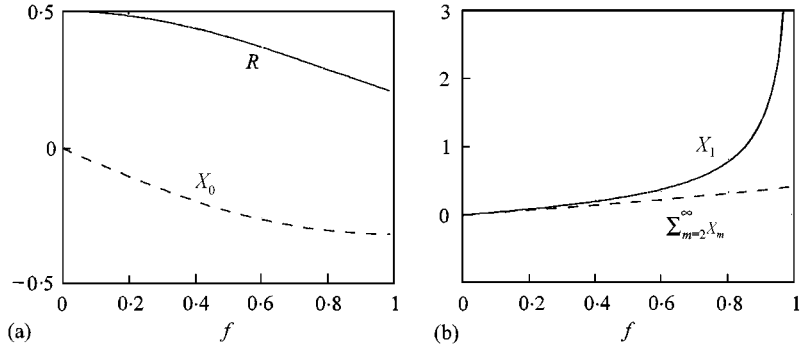

Figure 3. Radiation impedance for piston of $\alpha = 1$: (a) radiation resistance R and negative reactance from the plane wave mode X_0; (b) reactance from the evanescent waves, with contribution from the first mode, X_1, separated from the sum of the rest, $\sum_{m=2}^{\infty} X_m$.

3. The contribution of reactance from the plane wave mode is negative, $X_0 < 0$, which is unique to the confined geometry like the duct. It will be shown in later sections that the negative reactance may be maximized and utilized to extend the bandwidth of TL. The physics of the negative reactance is explained as follows.

Positive reactance can be interpreted either as positive virtual mass or negative virtual spring stiffness. The former is more frequently used due to the linear frequency dependency, $X \propto \omega V$, at the low-frequency limit, $\omega \to 0$. Virtual mass originates from the acceleration of fluids in immediate contact with the moving piston. For a baffled circular piston of radius r, the virtual mass is positive ($\rho_0 \frac{8}{3} r^3$ for $\omega \to 0$). The reason for $X_0 < 0$ in the duct geometry lies in the effect of the opposite rigid wall, which can be replaced by a mirror image of the real piston. The pressure exerted by the imaginary piston has two parts. The first is an evanescent wave which is always in-phase with the evanescent wave emanating from the real piston albeit being somewhat smaller in magnitude. The second part is a travelling wave which arrives at the surface of the real piston at a retarded time. This time delay, say Δt, gives rise to a component in-phase with piston deceleration, as illustrated below.

$$p_{image} \propto V e^{-i\omega\Delta t} = V \cos \omega\Delta t - \frac{dV}{dt} \frac{\sin \omega\Delta t}{\omega}.$$

The negative virtual mass is $\sin \omega\Delta t/\omega$. This result is in qualitative agreement with the remark given by Mechel [18] that the radiation reactance at low frequencies is always a spring type when a radiator acts in a small volume, as well as with the much earlier experimental observation by Ronneberger [19] that the imaginary part of an orifice impedance corresponds to a negative attached mass.

Physically, it would be easier to interpret the negative reactance as positive stiffness but the mass-like frequency dependency makes the negative virtual mass more consistent mathematically. Stiffness-like fluid loading is common in enclosed fluids but it differs from X_0, as illustrated below. Consider the reaction of a shallow air cavity to harmonic vibration of a piston (cf. Figure 1 replacing the membrane with a piston of length d). The pressure variation can be written as

$$\frac{dp}{dt} = c_0^2 \frac{d\rho}{dt}, \qquad \frac{d\rho}{dt} = -\rho_0 \frac{V}{h} \to p = -\rho_0 c_0^2 \frac{\eta}{h},$$

where $\eta = V/i\omega$ is the piston displacement. The stiffness of the air cavity is $-pd/\eta = \rho_0 c_0^2 d/h$, which is constant.

We now investigate the effect of the piston axial length d through changing α. The negative reactance given in equation (6) as a function of frequency, $X_0(\theta_0)$, where $\theta_0 = f\alpha\pi/2$, has valleys determined by

$$\frac{dX_0}{d\theta_0} = \alpha \frac{\cos \theta_0}{2\theta_0^3} [2\theta_0 \cos \theta_0 - \sin \theta_0] = 0$$

for which there are many roots of θ_0. However, the first valley appears where $\cos \theta_0 = 0$ is the deepest and is the only one within the range of frequency of our concern:

$$\theta_0 = \frac{\pi}{2}, \qquad [X_0]_{\min} = -\frac{\alpha}{\pi}$$

as shown in Figure 4(a) for four different values of α.

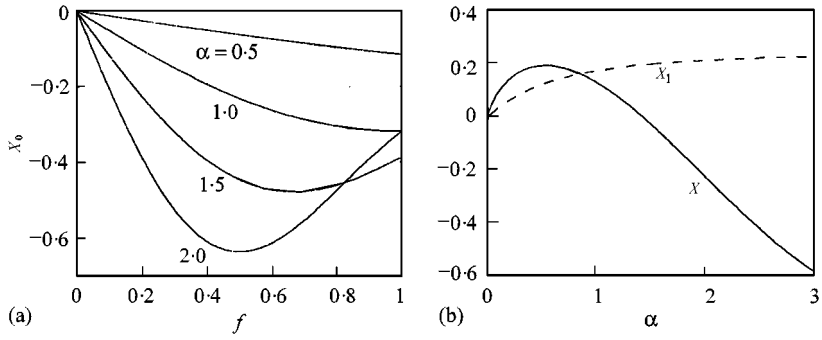

Figure 4. Effect of piston length on fluid reactance: (a) negative reactance from the plane wave mode for four values of α; (b) the total reactance (X) and first mode reactance (X_1) for a fixed frequency $f = 0{\cdot}35$.

For $\theta_0 = \pi/2$ the valley frequency is $f_v = \alpha^{-1}$. As α decreases, f_v shifts to a higher value and goes beyond the frequency band of (0, 1) when $\alpha < 1$. For small α, the segment of X_0 in $f \in (0, 1)$ is very linear; the reactance gives a nearly constant negative virtual mass and this will be shown later to have important consequences for TL. Figure 4(b) shows the variation of the first mode reactance and the total reactance for a fixed frequency of $f = 0{\cdot}35$. The total reactance becomes negative when α exceeds about 1·4.

2.3. LOADING ON THE NEIGHBOURING WALLS

The wave loading on the neighbouring walls within the source region, $|x| < d/2$, is needed when we study the effect of having identical pistons installed on these walls. As can be seen from equation (2), the loading on the opposite wall, $y = a$, is quite similar to that on the piston itself except for a factor of $\cos(m\pi y/a) = (-1)^m$. The average pressure on the opposite wall, $\bar{p}_a$, is written as

$$\bar{p}_a = \rho_0 c_0 V Z_a, \qquad Z_a = R + \mathrm{i} \sum_{m=0}^{\infty} (-1)^m X_m, \tag{7}$$

where R and X_m are the same as those given in equation (6). The loading on the corresponding areas on the side walls, $z = 0, b$, is calculated by integrating the pressure in both axial and vertical directions. The vertical integration

$$\int_0^a \cos\left(\frac{m\pi y}{a}\right) \mathrm{d}y = a \frac{\sin(m\pi)}{m\pi} = \begin{cases} a, & m = 0, \\ 0, & m \neq 0 \end{cases}$$

shows that there is contribution only from the plane wave. Similarly, we denote the average pressure on the side walls as $\bar{p}_b$:

$$\bar{p}_b = \rho_0 c_0 V Z_b, \qquad Z_b = Z_0 = R + \mathrm{i} X_0. \tag{8}$$

3. DYNAMICS OF A SINGLE MUFFLER

3.1. RESPONSE OF PISTON TO INCIDENT WAVES

We now calculate how a piston actually vibrates for a given plane incident wave leaving control of noise of higher modes to future studies. Note that even for plane incident waves,

the piston excites non-propagating higher order duct modes which have to be accounted for when calculating the piston response. Assuming the incident wave as $p_i = p_{i0}e^{-i\omega x/c_0}$, where p_{i0} is the wave pressure at $x = 0$, the loading on a rigid piston, as tactically assumed in the previous section, is expressed in terms of an average wave pressure $\bar{p}_w$ normalized by p_{i0}:

$$\frac{\bar{p}_w}{p_{i0}} = \frac{1}{d}\int_{-d/2}^{+d/2} e^{-i\omega x/c_0}\,dx = \frac{\sin\theta_0}{\theta_0}. \tag{9}$$

If the piston response is $V = V_0 e^{i\omega t}$, then its radiation fluid-loading is the same as that found earlier, $\rho_0 c_0 V Z$, where the radiation impedance Z is given in equation (6). The complete dynamics of the piston vibration can be written as

$$\bar{p}_w + \rho_0 c_0 V Z + K^* V/i\omega + D^* V + M^* i\omega V = 0, \tag{10}$$

where M^*, D^*, K^* are, respectively, the piston mass per unit area, structural damping and spring stiffness. Inserting $\bar{p}_w$ of equation (9), we have the response of the piston

$$\frac{\rho_0 c_0 V}{p_{i0}} = \frac{-\sin\theta_0/\theta_0}{Z + \mathscr{L}}, \tag{11}$$

where $\mathscr{L}$ is the structural dynamics operator involving mainly time derivatives

$$\mathscr{L} = M i\varpi + D + K/i\varpi, \tag{12}$$

$\varpi = \omega a/c_0$ is the normalized angular frequency defined earlier, and M, D, K are, respectively, the normalized piston mass, damping and spring stiffness given as

$$M = \frac{M^*}{\rho_0 a}, \qquad D = \frac{D^*}{\rho_0 c_0}, \qquad K = \frac{K^* a}{\rho_0 c_0^2}. \tag{13}$$

3.2. TRANSMISSION LOSS AND PRESSURE RELEASE

The farfield pressure is derived from equation (4) by letting $|x| \to +\infty$:

$$p \pm = \rho_0 c_0 \left[\frac{\alpha}{2}\frac{\sin\theta_0}{\theta_0}\right] V_0 e^{i\omega(t \mp x/c_0)},$$

where signs $\pm$ are for downstream and upstream travelling waves respectively. Inserting V from equation (11) and together with R from equation (6), we get

$$\frac{p_\pm}{p_i} = \frac{-R}{Z + \mathscr{L}}. \tag{14}$$

Conservation of sound energy can be checked as follows:

$$|p_i|^2 = |p_i + p_+|^2 + |p_-|^2 \to 1 = \left|1 + \frac{p_+}{p_i}\right|^2 + \left|\frac{p_-}{p_i}\right|^2 \to$$

$$1 = \left|1 - \frac{R}{Z + \mathscr{L}}\right|^2 + \left|\frac{R}{Z + \mathscr{L}}\right|^2 \to |Z + \mathscr{L}|^2 = |iX + \mathscr{L}|^2 + R^2.$$

The last equation holds when $\mathscr{L}$ has zero real part, i.e., no damping. TL is found as follows:

$$\mathrm{TL} = 20\log_{10}\left|\frac{p_i}{p_+ + p_i}\right| = 20\log_{10}\left|\frac{Z+\mathscr{L}}{\mathrm{i}X+\mathscr{L}}\right|. \tag{15}$$

To check this result, we consider hard or heavy pistons, for which $|\mathscr{L}| \gg |Z|$, TL = 0, no TL occurs, as expected.

Equation (15) shows that $\mathrm{TL} \to \infty$ when $\mathrm{i}X + \mathscr{L} = 0$. This condition corresponds to total wave reflection or complete pressure release. Leaving the effect of structural damping to later discussions by assuming $D = 0$, this condition becomes

$$X + M\varpi - K/\varpi = 0 \tag{16}$$

and the forced piston vibration is, from equation (11),

$$V = -\frac{p_{i0}}{\rho_0 c_0}\left[\frac{\alpha}{2}\frac{\sin\theta_0}{\theta_0}\right]^{-1}.$$

For compact piston, $d \to 0$, we have $\theta_0 \to 0$, $Vd/2 = -a(p_{i0}/\rho_0 c_0)$, which means that half of the volume velocity caused by the piston oscillation just cancels that of the incident wave. Such a finite response can hardly be regarded as resonance, the use of which is in fact associated with the condition of forced oscillation without radiation resistance. But "resonance" will be used in the following text to describe such a condition interchangeably with 'complete pressure release' or simply 'pressure release'.

If we treat the radiation reactance as virtual mass, $M_v = X/\varpi$, which is normally frequency-dependent, the condition of pressure-release for a frictionless system, equation (16) becomes

$$(M_v + M)\varpi = K/\varpi,$$

which is simply a condition for piston 'resonance' at angular frequency ϖ taking virtual mass into consideration. TL for a very light and frictionless piston having *in vacuo* resonance at $f_0 = \pi^{-1}\sqrt{K/M} = \pi^{-1}\sqrt{0{\cdot}3/0{\cdot}15} = 0{\cdot}45$ is shown in Figure 5.

The actual resonance frequency is $f_{res} = 0{\cdot}34$. As frequency moves away from that of resonance, TL falls rapidly. For lower frequency, $f < f_{res}$, this is caused by the magnitude of

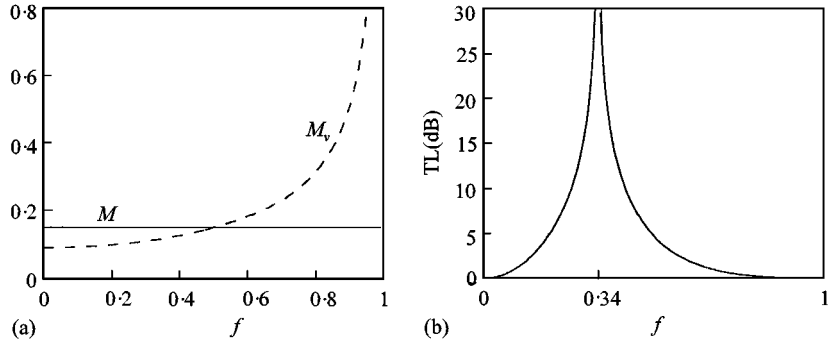

Figure 5. The transmission loss caused by a frictionless piston of $M = 0{\cdot}15$, $K = 0{\cdot}3$: (a) comparison of the piston mass with the virtual mass of fluid loading; (b) the transmission loss showing complete sound reflection at the shifted resonance frequency of $f = 0{\cdot}34$.

the stiffness term $K/\mathrm{i}\varpi$ which makes $|\mathscr{L}| \gg |Z|$, and TL given in equation (15) vanishes. For higher frequency, it is caused by the soaring virtual mass, $X \gg |\mathscr{L}|$, TL $\to 0$, and to a lesser extent by the inability of the piston to radiate sound [cf. Figure 3(a) for radiation resistance]. The strategy of creating a wide stopband is now clear. First, the structural stiffness has to be minimized in order to boost TL in the low-frequency region. Second, the piston has to be light so that the resonance peak is moved towards higher frequencies. By stating the second point we recognize the fact that the virtual mass tends to infinity near the first cut-on frequency and there is nothing we can do to prevent the rapid fall-off of TL beyond f_{res}. Since there is a practical limit to how light a piston can be, we need to utilize the negative reactance provided by the piston vibration to achieve the smallest possible total mass.

3.3. PERFORMANCE OF A SINGLE COMPLIANT PISTON

As shown in Figure 4(b), a relatively long piston has the chance of achieving negative virtual mass or positive virtual spring, $\alpha > 1{\cdot}4$ for frequency $f = 0{\cdot}35$ in that figure. We now investigate the effects of negative reactance by assuming that the structural stiffness K can be made to vanish by magnetic arrangement. A completely limp piston ($K = 0$) will obviously be unstable but we temporarily set $K = D = 0$ for the sake of clarity, leaving the effects of $K > 0$, $D > 0$ to later discussions. The performance of such an ideal piston of $\alpha = 2$ is shown in Figure 6(b) for three values of piston mass $M = 0{\cdot}1$, $0{\cdot}2$, $0{\cdot}3$.

Comparing with the performance of the earlier piston of $K = 0{\cdot}3$ shown in Figure 5(b), we see an extra resonance peak at $f = 0$, which is achieved by $K = 0$ and explained as follows. For a completely limp and frictionless piston, we have $\mathscr{L} = M\mathrm{i}\varpi$, which vanishes when $f \to 0$, so does the fluid reactance X, either positive or negative. But the radiation resistance $R = \alpha/2$ when $f = 0$. Equation (15) then gives $\mathrm{TL}|_{f\to 0} \to \infty$.

We now investigate the second resonance peak at $f = 0{\cdot}36$ for a piston of $M = 0{\cdot}2$. Figure 6(a) is the plot of the negative reactance, $-X$, together with the structural inertia, $M\varpi$, and the two match at $f = 0{\cdot}36$. One way to view $-X$ is negative virtual mass, which completely neutralizes the positive structural inertia at $f = 0{\cdot}36$. The other is positive virtual stiffness which, in this case, is strongly frequency-dependent. The virtual stiffness and the real piston mass give the second resonance at $f = 0{\cdot}36$ in addition to that at $f = 0$. The decrease of TL between the two resonance peaks shown in the middle curve of Figure 6(b) is caused by the

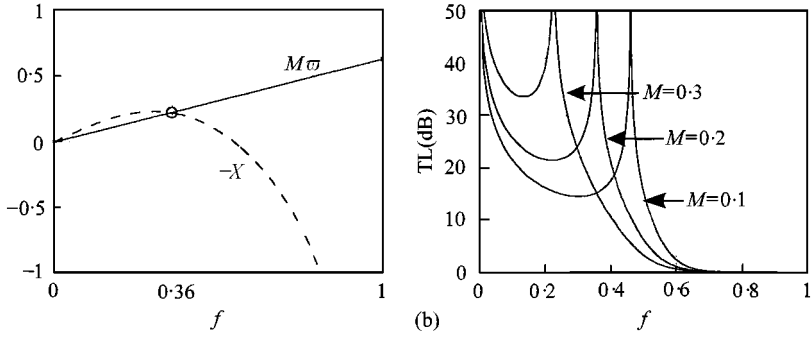

Figure 6. Transmission loss for a light piston of $\alpha = 2$, $K = D = 0$ showing two resonance peaks including one at $f = 0$: (a) comparison of piston inertia $M\varpi$ with the negative reactance, $-X$, for $M = 0{\cdot}2$; (b) TL for $M = 0{\cdot}1$, $0{\cdot}2$, $0{\cdot}3$ illustrating the trade-off between bandwidth and level of transmission loss.

gap between $-X$ and $M\varpi$ shown in Figure 6(a). TL beyond f_{res} falls rapidly because of the diverging positive reactance caused by the first mode contribution, $X_{f\to 1}\to\infty$.

In Figure 6(b), comparison of performance is made among pistons with $M = 0{\cdot}1, 0{\cdot}2, 0{\cdot}3$, for which the second resonance peaks are at $f = 0{\cdot}46, 0{\cdot}36, 0{\cdot}23$ respectively. There is a clear trade-off between the useful frequency bandwidth and the level of TL. A somewhat arbitrary design criterion may be set by choosing the piston mass to neutralize the virtual negative mass at the peak of negative reactance ($-X$). It can be seen from Figure 6(a) that $M = 0{\cdot}2$ roughly satisfies this criterion and the lowest TL achieved in the suspension-bridge-like region is over 20 dB, a level which can only be achieved with an ideal expansion chamber of area ratio 20·0 at the resonance frequency.

4. DUAL AND QUADRUPLE PISTON SYSTEMS

4.1. DYNAMICS OF PISTON IN PAIRS

Having understood that the soaring virtual mass at higher frequencies is responsible for the rapid deterioration of TL, we introduce another piston at the opposite wall, $y = a$. The reciprocity principle tells us that the pressure at $y = 0$ caused by the extra piston is the same as the pressure at $y = a$ radiated by the piston at $y = 0$, which is given as $\bar{p}_a$ in equation (7), provided that the two piston vibrations are symmetrical in the sense that they push into and withdraw from the duct simultaneously. Z_a of equation (7) may be called the mutual impedance. It has alternating signs for successive modes. The contribution from all odd modes is absent from the total impedance of the piston acting in pair:

$$Z + Z_a = 2\left(R + \mathrm{i}\sum_{m=0,2,4,\cdots} X_m\right). \tag{17}$$

The reactance is now much reduced due to (a) the absence of the dominating X_1 and (b) the doubling of the negative reactance X_0.

We now check the symmetry assumption. In analogy with the dynamics of a single piston, equation (10), we write the normalized version for the two pistons identified by subscripts 1 and 2, respectively, as

$$\bar{p}_w/\rho_0 c_0 + (V_1 Z + Z_a V_2) + \mathscr{L}_1 V_1 = 0,$$

$$\bar{p}_w/\rho_0 c_0 + (V_2 Z + Z_a V_1) + \mathscr{L}_2 V_2 = 0,$$

which may be solved for V_1, V_2 as follows:

$$V_1 = -\frac{\bar{p}_w}{\rho_0 c_0}\left[\frac{\mathscr{L}_2 + Z - Z_a}{(\mathscr{L}_1 + Z)(\mathscr{L}_2 + Z) - Z_a^2}\right],$$

$$V_2 = -\frac{\bar{p}_w}{\rho_0 c_0}\left[\frac{\mathscr{L}_1 + Z - Z_a}{(\mathscr{L}_1 + Z)(\mathscr{L}_2 + Z) - Z_a^2}\right].$$

If the two pistons are identical, $\mathscr{L}_1 = \mathscr{L}_2 = \mathscr{L}$, we have

$$V_1 = V_2 = -\frac{\bar{p}_w}{\rho_0 c_0}\left[\frac{1}{\mathscr{L} + Z + Z_a}\right]$$

as expected. The two pistons radiate into the far fields identical plane waves with total pressure p_+, the total transmission coefficient being

$$\left.\frac{p_+}{p_i}\right|_{dual} = \frac{-2R}{Z + Z_a + \mathscr{L}}$$

following the procedures leading to equation (14). The corresponding TL is

$$\mathrm{TL}_2 = 20\log_{10}\left|\frac{Z + Z_a + \mathscr{L}}{\mathrm{i}\,\mathrm{Im}(Z + Z_a) + \mathscr{L}}\right| \tag{18}$$

in which $\mathrm{Re}(Z) = \mathrm{Re}(Z_a) = R$ has been used and $(Z + Z_a)$ is given in equation (17).

Similarly, for four identical pistons installed on the four walls of a square duct,

$$\mathrm{TL}_4 = 20\log_{10}\left|\frac{Z + Z_a + 2Z_b + \mathscr{L}}{\mathrm{i}\,\mathrm{Im}(Z + Z_a + 2Z_b) + \mathscr{L}}\right|. \tag{19}$$

The extra benefit of introducing the pair of side-wall pistons is that the mutual impedance $Z_b = Z_0$ has no positive reactance component at all [cf. equation (8)]. Thinking along this line, one might have wondered whether a piston in the form of a circular ring in a circular tube could produce the highest possible negative fluid reactance, but surely the physics would not have been made so clear had we started with the circular geometry.

The negative reactances for the dual and quadruple piston systems are plotted in Figure 7 for different piston aspect ratios in a square duct.

It can be seen that both dual and quadruple piston systems exhibit negative reactance for the whole plane wave frequency range, and the magnitude of X in the quadruple system is about twice as large as that of the dual system. Also, notice that for a large aspect ratio X has a parabola-like curve and has a negative peak within the frequency range. For low aspect ratio systems, however, $X(f)$ takes the linear section and will neutralize $M\varpi$ more effectively, which is the key to raising the lowest TL level between the two resonance peaks. The problem in using short pistons, however, is the low magnitude of negative reactance

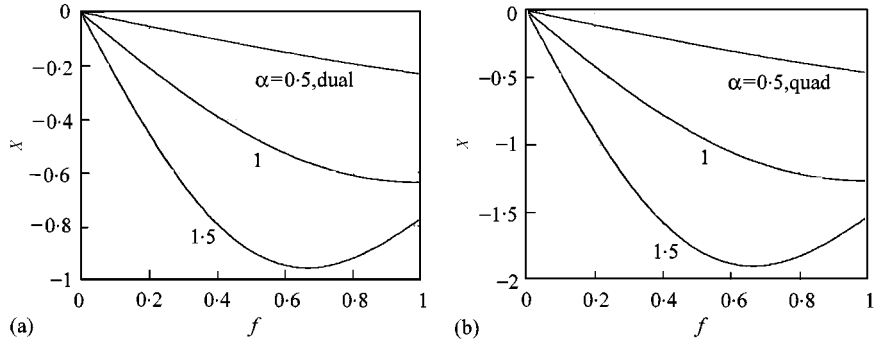

Figure 7. Total reactance of (a) dual and (b) quadruple piston systems for aspect ratios of $\alpha = 0{\cdot}5$, 1·0, 1·5.

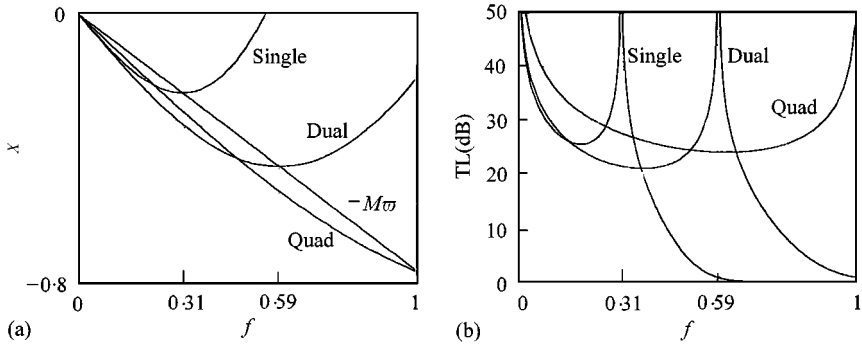

Figure 8. Comparison of TL for single, dual and quadruple pistons with equal mass of $M = 0{\cdot}24$. The aspect ratios are, respectively, $\alpha_1 = 2$, $\alpha_2 = 1{\cdot}26$, $\alpha_4 = 0{\cdot}68$. The single, dual and quadruple piston systems are, respectively, labelled "single", "dual" and "quad": (a) the matching between the structural inertia ($-M\varpi$, straight line) and the reactance; (b) TL spectra demonstrating that the performance of the dual piston system is better than the single piston while the quadruple system has high TL level for the whole bandwidth.

available, such that the piston mass may become unrealistically small, e.g., 10 μm, for applications of noise control in small ducts.

4.2. MINIMUM TL AND PISTON MASS

Since the low piston mass required is likely to be a crucial issue in implementation, we compare the performance by single, dual and quadruple pistons with the same mass. We first choose the piston aspect ratio $\alpha_1 = 2$ for the single piston and the mass is optimized by the criterion stated earlier to give $M_1 = 0{\cdot}24$. Then we iterate to find the piston aspect ratio $\alpha_2 = 1{\cdot}26$, $\alpha_4 = 0{\cdot}68$ for the dual and quadruple pistons so that $M_2 = M_4 = M_1$. The comparison of reactance-matching and TL spectra are plotted in Figure 8.

Figure 8(b) shows that the TL bandwidth for the dual piston is almost twice as wide as that of the single piston with a comparable TL level. For the quadruple system, however, the valley of reactance is beyond the frequency band under consideration, and the reactance-matching or resonance is set at $f = 1$. The lowest TL between the two resonance peaks is $\mathrm{TL}_{min} = 24{\cdot}1$ dB, 3 dB higher than that of the dual piston.

We now concentrate on dual and quadruple pistons and plot the optimized piston mass and TL_{min} achieved in the stopband in Figure 9.

The solid lines in Figure 9(b) are TL_{min} achieved in the stopband. The second resonance frequency is shown as the dashed lines based on the right-hand co-ordinate scale and is essentially the bandwidth. The combination of TL_{min} and f_{res} curves in Figure 9(b) illustrates that the quadruple system offers a wider bandwidth at the price of a lower TL_{min}. However, for $\alpha < 1$, the bandwidth for the quadruple system extends to the whole plane wave range and the level of TL_{min} is very high, which is impossible for the dual piston.

Figure 9(a) shows that the structural mass for the quadruple piston is typically twice as much as that for the dual piston system. The reason is that a much higher negative reactance is available in the former to balance out the positive structural inertia. Since such a low structural mass may not be easy to implement, the quadruple system has the advantage of being more practical. The mass level for the dual piston system approaches zero as $\alpha \to 0{\cdot}64$ from above since there is no negative reactance available to make a resonance below that α.

Focusing on the quadruple system, we see an extraordinary performance for $\alpha < 1$. The low-mass requirement is relaxed when α increases beyond unity when the second resonance

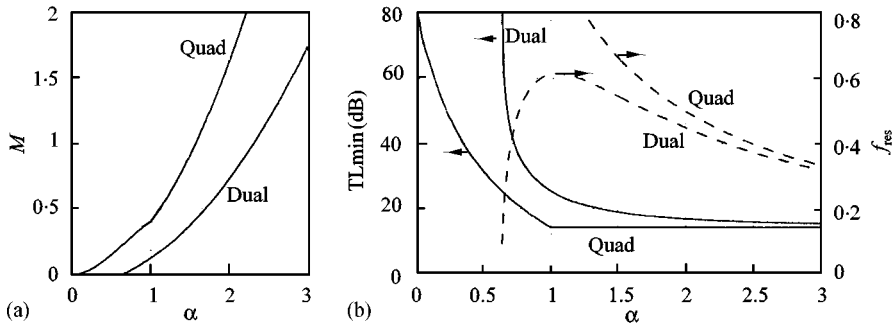

Figure 9. Performance of dual and quadruple pistons used as duct noise muffler: (a) the optimized piston mass; (b) TL_{min} between the two resonance peaks (solid lines based on the left-hand co-ordinate scale) and the second resonance frequency (dashed lines based on the right-hand co-ordinate scale). The labels on curves are identical to those of the previous figure.

peak appears in the plane wave range similar to the dual piston system. An interesting phenomenon of plateau occurs at $TL_{min} = 14{\cdot}2$ dB [see Figure 9(b)]. This level is certainly above what is achieved in low-frequency noise control by either passive or active means. The important implication is that increasing the piston aspect ratio can ease the otherwise stringent requirement for light structural material. For example, as shown in Figure 9, the quadruple system of $a = 1{\cdot}5$ has the optimal mass $M = 0{\cdot}91$. Its performance is a TL higher than 14·2 dB for frequency from zero to the resonance peak at $f_{res} = 0{\cdot}67$. Taking air density as $1{\cdot}225\ \mathrm{kg/m^3}$ and the isentropic speed of sound as 340 m/s, a square duct of height $a = 0{\cdot}3$ m has the first cut-on frequency $c_0/2a \approx 567$ Hz, hence $f^*_{res} = 380{\cdot}0$ Hz. The optimal mass per unit area of

$$M^* = M(\rho_0 a) = 0{\cdot}91 \times (1{\cdot}225 \times 0{\cdot}3) = 0{\cdot}33\ \mathrm{kg/m^2},$$

which is equivalent to 43 μm thick metal foil of iron density. Depending on the magnetic strength required, it is also possible to use ferromagnetic powders deposited on a substrate made of other materials like aluminium alloy. In such a case the structure can afford to be even thicker. It therefore appears that the clamped membrane sketched in Figure 1 may be replaced by a piston on a spring support.

4.3. EFFECTS OF STRUCTURAL STIFFNESS AND DAMPING

We have so far ignored damping and assumed zero structural stiffness. We have demonstrated that the piston vibration induces positive virtual stiffness which helps to establish a second resonance peak in the TL spectrum. Since the virtual stiffness becomes zero at the DC frequency. Static stability demands a positive "residual" structural stiffness $K > 0$. The effects of this and of damping are now investigated. The ideal system is without damping and stiffness, and the piston mass is optimized for the broadest possible stopband as described earlier.

We first introduce $K = 0{\cdot}03$ as a typical residual structural stiffness. The performance of the system with residual stiffness is compared with that without residual stiffness in Figure 10 in which the two systems are marked "stiff" and "ideal" respectively.

Figure 10(a) is for a dual piston system while Figure 10(b) is for a quadruple piston system. For the dual piston of $\alpha = 1{\cdot}5$, the optimized mass is $M = 0{\cdot}38$. The main effect of

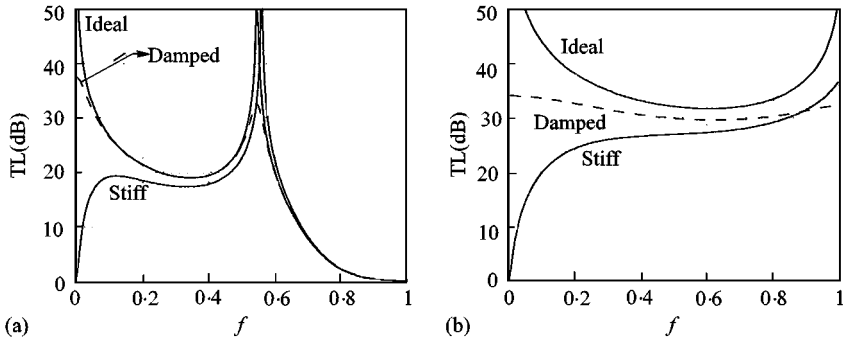

Figure 10. Effects of residual structural stiffness and damping on transmission loss. The ideal systems without damping and stiffness, that with damping of $D = 0{\cdot}02$ but no stiffness, and those without damping but with residual stiffness of $K = 0{\cdot}03$, are labelled 'ideal', 'damped' and 'stiff', respectively: (a) dual piston system with $\alpha = 1{\cdot}5$ and optimal mass $M = 0{\cdot}38$; (b) quadruple piston of $\alpha = 0{\cdot}5$ and optimal mass $M = 0{\cdot}15$.

the residual stiffness is the elimination of the first resonance peak at the DC frequency. But for the small value of residual stiffness chosen, the TL curve rises from the origin to a level comparable to the ideal system in a very short frequency band. In fact, there is a local maxima at $f = 0{\cdot}12$ and the lowest TL between this and the resonance peak at $f = 0{\cdot}55$ is 17·3 dB, compared with 19·0 dB of the ideal system. The effect on the quadruple piston of $\alpha = 0{\cdot}5$, $M = 0{\cdot}15$, shown in Figure 10(b), is larger over the whole frequency band. The ideal system has TL_{min} of 31·8 dB while the 'stiff' system does not show a local minima, but TL is reduced to 20 dB at $f = 0{\cdot}10$. Nevertheless, the conclusion can be drawn that a small positive structural stiffness may be allowed to maintain static stability without reducing the stopband significantly. The elimination of stopband near the DC frequency should not constitute a major concern for noise control.

To investigate the effect of structural damping we first estimate the range of damping coefficient define earlier, $D = D^*/\rho_0 c_0$. Assuming that the piston has an *in vacuo* dimensional eigenfrequency of

$$\omega_0 = \mathrm{i}\frac{D^*}{2M^*} \pm \sqrt{\frac{K^*}{M^*}},$$

the specific damping ($\bar{D}$), defined as the rate of amplitude reduction per oscillation cycle, is calculated as

$$\bar{D} = 1 - \mathrm{e}^{-\mathrm{Im}(\omega_0)[2\pi/\mathrm{Re}(\omega_0)]} \approx \frac{2\pi\,\mathrm{Im}(\omega_0)}{\mathrm{Re}(\omega_0)} = \frac{2\pi D^*}{2\sqrt{K^*M^*}} = \frac{\pi D}{\sqrt{KM}},$$

in which the definitions in equation (13) have been used. A typical value of $\bar{D}$ for metal is 0·005. For limp and light piston with $K = 0{\cdot}03$, $M = 0{\cdot}3$, we have $D = 1{\cdot}5 \times 10^{-4}$, which does not produce any noticeable change of TL spectrum apart from making the otherwise singular resonance peak finite. But for systems which are not so limp nor light, D could be a lot higher. We therefore choose $D = 0{\cdot}02$ to see the trend. The TL curves for the damped system (labelled 'damp') are plotted as dashed lines in Figure 10. We can see that the effect on the dual system is still very minor but for the quadruple system, TL of the damped pistons runs between the 'ideal' and 'stiff' lines with $\mathrm{TL}_{min} = 29{\cdot}6$ dB. In short, we conclude that the effect of damping is minor.

5. CONCLUSIONS

The concept of a compact device for controlling low-frequency duct noise is introduced. Theoretical analysis of the limiting case shows that high transmission loss can be maintained from the DC frequency to the first cut-on of the duct by using flush-mounted identical pistons on the four duct walls. The bandwidth narrows towards the middle ground when practical concerns of stability and structural mass are taken into account. But the performance shown in the calculated examples compares very well with that of an earlier active control system [20] which succeeded in creating an 'acoustic earth' condition with a TL reaching up to 20 dB at some resonance-like bands. Such performance is made possible by two factors which are absent in traditional Helmholtz-type mufflers.

The first factor is the introduction of magnetic attraction force between a ferromagnetic piston and a permanent magnet outside the duct. When the piston is displaced outwards, at the attraction force increases and tends to displace the piston further, rendering negative spring stiffness. When the negative stiffness neutralizes the positive stiffness of the mechanical support for the piston, the system has zero total structural stiffness and exhibits resonance behaviour at zero frequency where, theoretically, pressure-release condition is achieved and TL becomes infinity. In practice, a small allowance of positive stiffness has to be given to maintain static stability, but it does not seem to affect TL significantly except for a very narrow region near the DC frequency.

The second factor is the utilization of negative fluid reactance which is unique in the duct configuration and maximized by the design of identical pistons in pairs. The negative fluid reactance serves as a positive virtual stiffness for an otherwise completely limp piston, and a second pressure-releases or resonance condition is established at a finite frequency. The TL curve spans between the two resonance peaks resembling a suspension bridge with a minimum TL above 14·2 dB. Alternatively, one could view the negative reactance as a negative virtual mass which absorbs the structural inertia, enabling the limp piston responding to waves with only radiation resistance. Between the two resonance peaks the matching of the structural inertia and the negative reactance is not perfect as the negative reactance has a non-linear frequency dependency. But for light quadruple pistons, a rather linear segment of reactance is utilized and the system exhibits broadband pressure-release which has not been seen previously. The utilization of the negative fluid reactance is one of the focuses of this study, and the physics are summarized as follows.

First, vibration of a baffled piston produces only positive virtual mass together with radiation resistance. But the opposite wall in a duct has the effect of adding a mirror piston which also radiates travelling waves onto the real piston. These waves arrive at the real piston with a time delay and the delayed radiation resistance is transformed into negative reactance. The negative reactance from the travelling waves normally cancels only part of the positive reactance resulting from the evanescent waves surrounding the piston. The contribution of the first mode reactance approaches infinity as the excitation frequency approaches that of the first cut-on. This makes it impossible to achieve resonance close to the first cut-on frequency, however light the piston is. Indeed, we find the TL curve of a single-piston system as poor as a normal Helmholtz resonator at high frequencies and that the second resonance is typically limited to about half of the first cut-on frequency.

Second, an identical piston is introduced on the opposite wall of the duct to form a dual-piston system which vibrates in breathing mode. Each piston is subject to both self-induced radiation load and mutual fluid loading. The odd modes of the two loadings have anti-phase relationship and cancel each other, while the contributions from the even modes add up. The cancellation of the dominant first mode makes it possible to achieve very high negative reactance for the whole plane wave frequency range, and the doubling of

the radiation resistance further enhances the capability of the system to reflect incident waves. As a muffler, the dual-piston system performs much better than the single-piston system in terms of both TL level and bandwidth.

Along this line a quadruple piston system is used by installing another pair of pistons on the side walls. These pistons do not introduce any evanescent waves on the existing dual pistons, the only effect being the quadrupling of the plane wave mode impedance which consists of radiation resistance and negative reactance—the two essential ingredients for the success of a wave reflector. As a result, a typical quadruple system can easily extend the second reasonance frequency beyond the first cut-on, and the lowest TL value within the whole stopband is also dramatically raised. The structural mass that may be neutralized by the negative reactance is also increased to a level which is shown to be realistic in noise control applications. If in reality the pistons are replaced by short membranes for convenience of implementation, the excitation of structural modes [21, 22] will have to be taken into account.

ACKNOWLEDGMENTS

The author thanks Professor J. E. Ffowcs Williams for his kind help during the preparation of the manuscript, and the work was supported by a grant from the Research Grants Committee of the Hong Kong SAR (Grant No. PolyU 5127/98E).

REFERENCES

1. L. L. Beranek and I. L. Ver, Editors 1992 *Noise and Vibration Control Engineering*. New York: Wiley.
2. M. L. Munjal 1987 *Acoustics of Ducts and Mufflers*. New-York: Wiley-Interscience.
3. J. M. de Bedout, M. A. Franchek, R. J. Bernhard and L. Mongeau 1997 *Journal of Sound and Vibration* **202**, 109–123. Adaptive-passive noise control with self-tuning Helmholtz resonators.
4. Kh. Eghtesadi, W. K. W. Hong and H. G. Leventhall 1983 *Noise Control Engineering Journal* **20**, 16–20. The tight-coupled monopole active attenuator in a duct.
5. A. Roure 1985 *Journal of Sound and Vibration* **101**, 429–441. Self-adaptive broad-band active sound control system.
6. C. H. Hansen 1997 *Noise-Con 97 Proceedings, University Park, P. A. Book*, Vol. **2**, 3–38. Active noise control—from laboratory to industrial implementation.
7. A. H. Dowell 1975 *Aeroelasticity of Plates and Shells*. Leiden: Noordhoff International Publishing.
8. M. S. Howe 1982 *Journal of Fluid Mechanics* **125**, 59–73. On the instability of boundary-layer flow over a spring-mounted piston.
9. A. Cummings 1994 *Journal of Sound and Vibration* **174**, 433–450. The attenuation of sound in unlined ducts with flexible walls.
10. P. V. Bruel 1951 *Sound Insulation and Room Acoustics*. London: Chapman & Hall, Chapter 4.
11. R. D. Ford and M. A. McCormick 1969 *Journal of Sound and Vibration* **10**, 411–423. Panel sound absorbers.
12. W. Frommhold, H. V. Fuchs and S. Sheng 1994 *Journal of Sound and Vibration* **170**, 621–636. Acoustic performance of membrane absorbers.
13. K. Sakagami, M. Kiyama, M. Morimoto and D. Takahashi 1996 *Applied Acoustics* **49**, 237–247. Sound absorption of a cavity membrane: a step towards design method for membrane-type absorbers.
14. D. Takahashi, K. Sakagami and M. Morimoto 1996 *Journal of the Acoustical Society of America* **99**, 3003–3009. Acoustic properties of permeable membranes.
15. M. K. Hinders, B. A. Rhodes and T. M. Fang 1995 *Journal of Sound and Vibration* **185**, 219–246. Particle-loaded composites for acoustic anechoic coatings.

16. L. HUANG 1999 *Proceedings of the 6th International Congress on Sound and Vibration, Lyngby, Denmark*, 5–8 *July*, Vol. **1**, 449–454. Passive control of duct noise using magnetic forces.
17. P. E. DOAK 1973 *Journal of Sound and Vibration* **31**, 1–72. Excitation, transmission and radiation of sound from source distributions in hard-walled ducts of finite length (I): the effects of duct cross-section geometry and source distribution space–time pattern.
18. F.P. MECHEL 1988 *Journal of Sound and Vibration* **123**, 537–572. Notes on the radiation impedance, especially of piston-like radiators.
19. D. RONNEBERGER 1972 *Journal of Sound and Vibration* **24**, 133–150. The acoustical impedance of holes in the wall of flow ducts.
20. M. C. J. TRINDER and P. A. NELSON 1983 *Journal of Sound and Vibration* **89**, 95–105. Active noise control in finite length ducts.
21. K. S. SUM and J. PAN 1998 *Journal of the Acoustical Society of America* **103**, 1510–1519. A study of the medium frequency response of sound field in a panel-cavity system.
22. L. HUANG 1999 *Journal of the Acoustical Society of America* **106**, 1801–1809. A theoretical study of passive duct noise control by flexible panels.